Research article

Journal of RAMAN SPECTROSCOPY

Received: 12 October 2012 Revised: 14 November 2012 Accepted: 11 December 2012 Published online in Wiley Online Library: 14 March 2013

(wileyonlinelibrary.com) DOI 10.1002/jrs.4249

Study of carrier concentration profiles in Al-implanted Ge by micro-Raman spectroscopy under different excitation wavelengths

A. Sanson,[a]* M. Giarola,[b] E. Napolitani,[c] G. Impellizzeri,[d] V. Privitera,[d] A. Carnera[a] and G. Mariotto[b]

The distribution profile of Al implanted in crystalline Ge has been investigated by micro-Raman spectroscopy. Using different excitation laser lines, corresponding to different optical penetration depths, the Al concentration at different depths beneath the sample surface has been studied. We have found a strong correlation between the intensity of the Al–Ge Raman peak at ~370 cm^{-1}, which is due to the local vibrational mode of substitutional Al atoms, and the carrier concentration profile, obtained by the spreading resistance profiling analysis. A similar connection has been also observed for both shape and position of the Ge–Ge Raman peak at ~300 cm^{-1}. According to these experimental findings, we propose here a fast and nondestructive method, based on micro-Raman spectroscopy under different excitation wavelengths, to estimate the carrier concentration profiles in Al-implanted Ge. Copyright © 2013 John Wiley & Sons, Ltd.

Keywords: micro-Raman spectroscopy; carrier concentration; substitutional atoms; Ge doping; spreading resistance profiling

Introduction

Studies of the doping process, in terms of diffusion and electrical activation of the dopants, play a crucial role for the evolution of electronic technology. Among the techniques suitable for this kind of studies, a four-point probe combined to Hall measurements allows to obtain information on sheet resistance, carrier type and dose, together with the mobility of the carriers.[1] Spreading resistance profiling (SRP) analysis, instead, allows to extract the carrier concentration profile from resistivity measurements.[2] Unfortunately, this technique requires a complex and destructive sample preparation by a beveling procedure.

Micro-Raman spectroscopy is one of the most used techniques for studying the physico-chemical properties of semiconductor micro-structures and micro-devices. It is currently exploited for strain characterization, for determining the crystallinity degree in thin films and the local temperature in devices under operational conditions.[3–5] On the other hand, it is well known that for high doping levels, Si and Ge Raman peaks can be strongly affected by carrier concentration effects.[6] With this regard, few years ago, O'Reilly *et al.*[7] found a correlation between Si Raman shift and peak carrier concentration measured by differential Hall technique for Sb-implanted Si. Soon later, M. Becker *et al.*,[8] by combining micro-Ramam spectroscopy with small angle beveling preparation techniques, derived, in the framework of Fano resonance theory, a rough linear relationship between the reciprocal symmetry parameter of Si Raman peak and the free hole concentration. More recently, Perova and co-workers,[9,10] studying the structural damage in Ge wafers caused by hydrogen and helium implantation, found a correlation between Raman mapping measurements on beveled samples and SRP analysis. All these works show that, in principle, micro-Raman spectroscopy could be employed to characterize the carrier concentration profiles in crystalline semiconductors. However, up to now, micro-Raman spectroscopy was not used for these purposes because the technique in part is not yet refined for quantitative characterizations, and in part, when combined with beveling method, it is destructive too, thus resulting not particularly advantageous compared with the SRP technique.

In this work, Al-implanted Ge samples have been investigated by micro-Raman spectroscopy under excitation by some different laser lines. In the visible region, optical absorption coefficient of germanium is much higher than that of silicon, so that the light penetration length in Ge ranges approximately from 10 to 150 nm.[11] Therefore, by simply using laser lines of different wavelengths, we can straightforwardly probe the vibrational dynamics of implanted samples at different depths beneath the sample surface, without bevel of the sample surface. As will be shown in the succeeding text, the present approach, fast and nondestructive, allows us to estimate the carrier concentration profiles of dopant in Ge as a function of depth.

* *Correspondence to: A. Sanson, Dipartimento di Fisica e Astronomia 'G. Galilei', Università di Padova, Via Marzolo 8, I-35131, Padova, Italy. E-mail: andrea.sanson@unipd.it*

a *Dipartimento di Fisica e Astronomia 'G. Galilei', Università di Padova, Via Marzolo 8, I-35131, Padova, Italy*

b *Dipartimento di Informatica, Università di Verona, Strada Le Grazie 15, I-37134, Verona, Italy*

c *CNR-IMM MATIS at Dipartimento di Fisica e Astronomia, Università di Padova, Via Marzolo 8, I-35131 Padova, Italy*

d *CNR-IMM MATIS at Dipartimento di Fisica e Astronomia, Università di Catania, Via S. Sofia 64, I-95123 Catania, Italy*

Experimental details

Ge samples were prepared on Ge Czochralski (100) wafers, n-type Sb-doped with a resistivity higher than 40 Ω cm. Al ions were implanted with an energy of 25 keV and a fluence of 1×10^{15} Al/cm^2. After the implant (projected range ~25 nm), the samples were annealed at 400 °C for 1 h to induce the recrystallization of the Ge matrix by solid-phase epitaxy. Finally, four samples were further annealed for 1 h at 500, 600, 700, and 800 °C. According to Impellizzeri *et al.*,[14] above 600 °C, a strong electrical deactivation is observed by SRP measurements; an uphill diffusion toward the surface is detected by secondary ions mass spectrometry.

Polarized micro-Raman spectra were collected at room temperature in backscattering geometry using a triple monochromator (Horiba-Jobin Yvon, model T64000), set in double-subtractive/single configuration and equipped with holographic gratings having 1800 lines/mm. The scattered radiation, filtered by the fore double monochromator, was detected at the spectrometer output by a multichannel charge-coupled-device detector, with 1024 × 256 pixels, which was cooled by liquid nitrogen, The spectra were excited, in turn, by the 514.5, 568.2, and 647.1 nm lines of a mixed Ar–Kr ion gas laser focused onto a spot of 2 μm in size through the lens of a 100× microscope objective having a numerical aperture = 0.90). The laser power on the sample surface was constant during the measurements and fixed between 5 and 15 mW (depending on the laser line) to avoid thermal heating. A wave-number calibration of the spectrometer was made by exploiting the rotational Raman bands of the air as reference. To maximize the intensity of both Ge–Ge and Al–Ge Raman peaks, the Raman measurements were performed in crossed *xy* polarization (*x* and *y* electric field directions of the incident and scattered light, respectively) aligning a crystallographic axis of the sample along the *x*-direction (for more details, see Ref. [12]). Because the intensity of the Ge–Ge Raman peak turned out nearly unchanged with respect to implanted samples annealed at different temperature, we can infer that the residual implantation damage after solid-phase epitaxy is negligible, according to the findings of recent transmission electron microscope investigations on the same samples.[14] For each excitation wavelength, at least three spectra were recorded from three different regions on the surface of each sample, and they showed a very good reproducibility. The spectral resolution was better than 0.6 cm^{-1}/pixel.

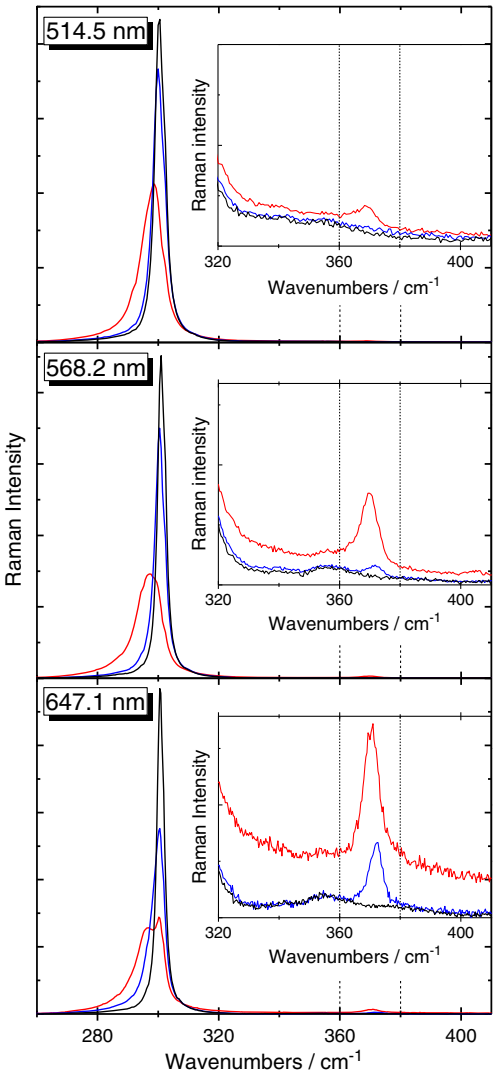

Figure 1. Raman spectra observed under excitation laser lines 514.5, 568.2, and 647.1 nm (top, middle, and bottom panel, respectively) in samples annealed at 400 and 400 °C + 700 °C (red and blue lines, respectively). Black lines are the Raman spectra collected in pure germanium here used as reference. The spectra are normalized to the area of the Ge–Ge peak at ~300 cm^{-1}. In the insets, the vertical scale was magnified 70 times in order to evidence the Al–Ge Raman peak at ~370 cm^{-1}. This figure is available in colour online at wileyonlinelibrary.com/journal/jrs

Results and discussion

Al–Ge Raman peak

Typical micro-Raman spectra of two selected samples (i.e. 400 and 700 °C), recorded in crossed polarization under excitation of the three different excitation laser lines, are shown in Fig. 1. All the Raman spectra display a very strong peak at about 300 cm^{-1}, because of the expected transverse optical phonon-mode of germanium with F_{2g} symmetry, and a much weaker, but much more important in this contest, peak at about 370 cm^{-1}, the intensity of which changes with the annealing temperature and laser wavelength. On the basis of the results of our recent Raman study on Al-implanted Ge,[12] this peak can be attributed to the local vibrational mode of substitutional Al atoms in the Ge matrix. Accordingly, indicating with $P(x)$ the density of substitutional Al atoms as a function of the depth x beneath the sample surface, the intensity of the Al–Ge Raman peak at ~370 cm^{-1}, measured at the laser wavelength λ_i, is proportional to the integral

$$X(\lambda_i) = \int_0^{+\infty} P(x) e^{-2x/L(\lambda_i)} dx \qquad (1)$$

where $L(\lambda_i)$ is the corresponding optical absorption length (i.e. the length in which the intensity of the light is reduced by a factor e^{-1}) and the term $e^{-2x/L(\lambda_i)}$ takes into account of the absorption of both the incident and scattered light. From Ref.,[11] we have estimated the values for $L(\lambda_i)$, which are about 17, 25, and 80 nm for the laser lines at 514.5, 568.2, and 647.1 nm, respectively.

For each sample and laser wavelength, we have calculated the aforementioned integral using, as $P(x)$ distribution, the carrier concentration profiles (here labeled $P_{SRP}(x)$) obtained by the SRP analysis reported in Ref.[14]. Subsequently, the relative

Journal of RAMAN SPECTROSCOPY

intensity of the Al–Ge Raman peak, calculated as the area[15] of the Al–Ge peak normalized to the area of the adjacent Ge–Ge Raman peak (which provides a reliable, although not absolute, internal reference), has been plotted *versus* the values obtained for integral (1), as it is shown in Fig. 2. This figure clearly suggests the occurrence of a linear relationship between the relative intensity of the Al–Ge peak and values of integrals (1). If the same calculation procedure is repeated using, as $P(x)$ distribution, the chemical Al–profiles obtained by the secondary ions mass spectrometry measurements reported in Ref.,[14] no similar correlation is obtained. Accordingly, we can infer that the substitutional Al atoms provide the entire amount of the electrically active carriers. Other possible contributions, for example those due to the presence of defects,[16] can be considered negligible. Therefore, we can claim that the relative intensity of Al–Ge Raman peak constitutes a reliable tool for a first rough estimation of the carrier concentration profiles, i.e. of the distribution of substitutional Al atoms in the Ge matrix.

Ge–Ge Raman peak

Let us now analyze the Ge–Ge Raman band peaked at ~300 cm^{-1}, whose average position, full width at half maximum (FWHM), and skew parameter (which is a measure of the peak asymmetry) have been calculated, with respect to pure Ge, for each sample and each excitation laser line, and plotted in Fig. 3 *versus* the corresponding amount of substitutional Al atoms, straightforwardly related to intensity of the Al–Ge Raman peak at ~370 cm^{-1}, as previously discussed.

In view of their plotting, the values of peak position, FWHM, and skew parameter were preliminarily normalized to the values of corresponding spectral features for unimplanted Ge, derived from Raman spectra recorded under the same experimental conditions, i.e. laser power at the sample surface and excitation wavelength. It can be observed, from the results shown in Fig. 3, that the spectral features (i.e., average position, FWHM, and skew parameter) characterizing the Ge–Ge Raman band of implanted samples progressively deviate from the reference values of pure Ge peak *versus* the increase of the Al–Ge Raman peak intensity. The measurements performed with the 647.1 nm laser line (full symbols in Fig. 3), corresponding to the highest optical penetration depth, show an appreciable deviation from the linear behavior due to the spurious contribution from the Ge substrate. In spite of this, the figure clearly shows the existence of a net correlation between the behavior of spectral features of the Ge–Ge Raman peak and the relative intensity of the Al–Ge Raman peak, i.e. between the spectral evolution Ge–Ge Raman peak and content of substitutional Al atoms in implanted samples.

It is well known that shape and position of the Raman peak can be influenced by the presence of phonon confinement,[17]

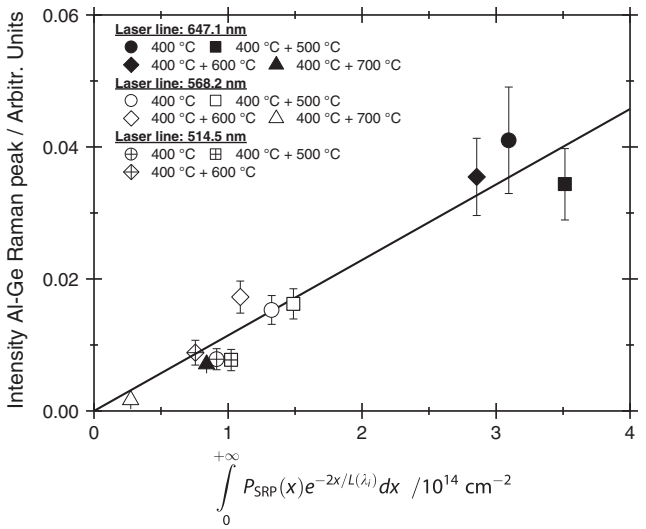

Figure 2. Intensity of the Al–Ge Raman peak at ~370 cm^{-1} plotted against and the carrier concentration profiles, probed by Raman, estimated by the spreading resistance profiles. Full, open, and cross symbols refer to the excitation laser lines 647.1, 568.2, and 514.5 nm, respectively. Circles, squares, diamonds, and up-triangles refer to the samples annealed at 400, 500, 600, and 700 °C, respectively. Owing to their very low content of substitutional Al atoms, the Al–Ge Raman peak was not observed for the sample annealed at 800 °C, as well as for the sample at 700 °C measured under the 514.5 nm laser line.

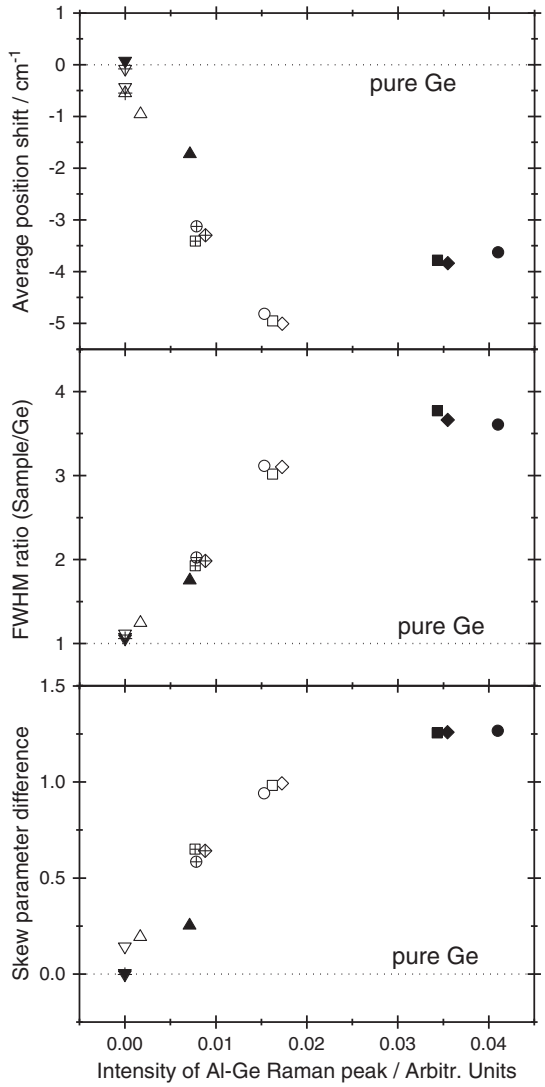

Figure 3. Average position (top panel), FWHM (middle panel), and skew parameter (bottom panel) of the Ge–Ge Raman peak at ~300 cm^{-1} (with respect to pure Ge), plotted against the corresponding intensity of the Al–Ge peak at ~370 cm^{-1}. The values were calculated with respect to the Ge–Ge peak of pure Ge measured under the same laser line. Symbols are the same as in Fig. 2, with the addition of down-triangles for the sample annealed at 800 °C. A direct correlation between Ge–Ge and Al–Ge Raman peaks is evinced.

strain[18] or, in the case of high doping concentrations, carrier concentration effects.[6] For example, regarding this last point, O'Reilly *et al.*[7] claimed that caution must be taken in the use of micro-Raman spectroscopy for strain characterization of highly doped and strained Si wafers.

In the present study, possible effects of phonon confinement on the Ge–Ge Raman peak can be neglected according to the results of transmission electron microscope investigations, which ruled out the existence of Ge nanocrystalline regions or clusters.[14] Concerning the lattice strain, this generally does not exceed a few tenths of percent in implanted and annealed samples, also in the case of high doping level.[19,20] In support of this statement, high resolution x-ray diffraction showed a lattice strain in our Al-implanted Ge samples (not shown) lower than 0.03% in the entire depth range.[13] This leads, according to Peng *et al.*,[21] to a shift and broadening of the Ge–Ge Raman peak much smaller than those reported in Fig. 3. Consequently, we can consider the shift and broadening of the Ge–Ge Raman peak shown in Fig. 3 entirely because of local concentration of substitutional Al atoms. Thus, the Ge–Ge Raman peak could be used to obtain quickly the information on the carrier concentration profiles, especially for the cases in which the Raman spectrum due to local vibrational modes of dopant atoms is not observed.

Simulation of the carrier concentration profile

On the basis of the aforementioned results, we are now interested to propose a method to reconstruct the carrier concentration profile from the Ge–Ge Raman peak. The same approach could also be suggested for the Al–Ge Raman peak, but because of its lower intensity, it turns out much more convenient to work on Ge–Ge Raman peak.

Figure 4 shows the FWHM and skew parameter of the Ge–Ge peak plotted as a function of integral (1), calculated, for each sample and excitation wavelength, using, as $P(x)$ distribution, the corresponding SRP given in Ref.[14]. The correlation between Ge–Ge Raman peak and carrier concentration profile, obtained by SRP analysis, is clearly evident.

The connection turns out even more strengthened by the fit of the experimental data of Fig. 4, which provides two average functions for the FWHM and skew parameter, i.e. the two solid lines in Fig. 4, which were labeled as g_σ and g_β, respectively. Starting from an arbitrary $P(x)$ distribution, we calculate the integral (1) for each of the n laser wavelengths used, i.e. λ_i, $i=1,..,n$ (in the present study, $n=3$). Hence, $g_\sigma[X(\lambda_i)]$ and $g_\beta[X(\lambda_i)]$ give an estimation of the FWHM and skew parameter of the Ge–Ge Raman peak, respectively, for the given $P(x)$ distribution measured with the ith laser line. By means of a Monte Carlo procedure, the $P(x)$ distribution is then varied in order to optimize, for each laser line, the agreement between the experimentally derived values and the estimated for both the FWHM and the skew parameter, i.e. so that to minimize the quantity

$$\sum_{i=1}^{n}\left[\frac{g_\sigma[X(\lambda_i)]-\sigma_i}{\sigma_i}\right]^2+\left[\frac{g_\beta[X(\lambda_i)]-\beta_i}{\beta_i}\right]^2 \qquad (2)$$

where σ_i and β_i are the experimental FWHM and skew parameter, respectively, obtained with the ith laser line. For the sake of comparison, Fig. 5 shows the resulting simulated $P(x)$ distribution obtained for the sample annealed at 500 °C and the carrier concentration profile from SRP measurements on the same sample. The agreement between Raman and SRP results is very good up to a depth of ~80 nm, i.e. within the optical penetration length of the laser line at 647.1 nm, where the carrier concentration is higher than 10^{18} cm^{-3}. In conclusion, the sharp correspondence between the simulated and the experimental spreading resistance profile makes us confident that micro-Raman spectroscopy under different excitation wavelengths could be used

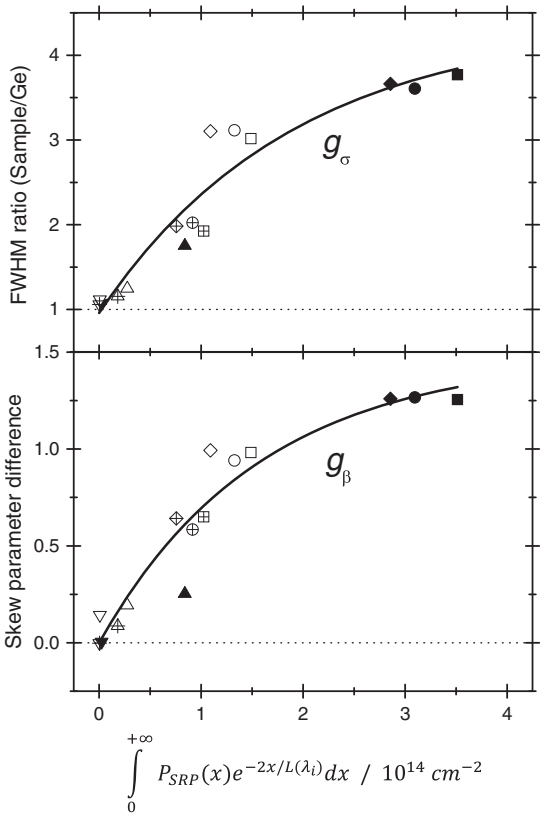

Figure 4. FWHM (top panel) and skew parameter (bottom panel) of the Ge–Ge Raman peak at ~300 cm^{-1} plotted against the integral of the carrier concentration profiles measured by spreading resistance profiling. The solid lines are the average functions g_σ and g_β used in the fitting procedure described in the text. Symbols are the same as in Fig. 2, with the addition of down-triangles for the sample annealed at 800 °C.

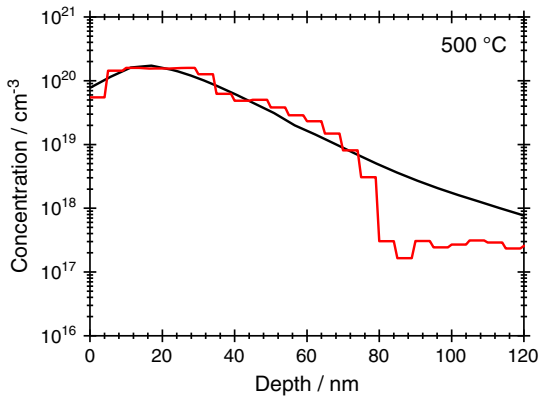

Figure 5. Comparison between carrier concentration profile measured by spreading resistance profiling (black line) and simulated profile obtained from the Ge–Ge Raman peak (red line). This figure is available in colour online at wileyonlinelibrary.com/journal/jrs

Journal of RAMAN SPECTROSCOPY

for a quantitative characterization of the doping species in Ge, at least in the range of the maximum optical absorption length and for high carrier concentration.

Conclusions

In this work, a micro-Raman spectroscopy investigation has been performed in Al-implanted Ge samples. By exploiting the optical penetration depths of different excitation wavelengths, we have studied the implanted Ge samples at different depths beneath the sample surface. A sharp correlation between the intensity of the Al–Ge Raman peak at ~370 cm^{-1}, related to substitutional Al atoms, and the carrier concentration profile, measured by SRP, has been found. A similar correlation has been derived also for both the shape and position of the Ge–Ge Raman peak at ~300 cm^{-1}. Accordingly, we propose a method, based on the Monte Carlo procedure, to determine the carrier concentration profiles starting from the spectral features of Ge–Ge Raman peak. Although additional studies are unavoidable in order to improve the efficiency of this method, the present work shows that micro-Raman spectroscopy under diverse excitation wavelengths can be used as a fast and nondestructive technique for a quantitative evaluation of the carrier profiles in Ge.

References

[1] L. J. Van der Pauw. *Philips Res. Report*, **1958**; *13*, 1.
[2] T. Clarysse, P. De Wolf, H. Bender, W. Vandervorst. *J. Vac. Sci. Technol. B* **1996**; *14*, 358.
[3] P. H. Tan, K. Brunner, D. Bougeard, G. Abstreiter. *Phys. Rev. B* **2003**; *68*, 125302.
[4] G. Kolb, T. Salbert, G. Abstreiter. *J. Appl. Phys.*, **1991**; *69*, 3387.
[5] R. Aubry, C. Dua, J. C. Jacquet, F. Lemaire, P. Galtier, B. Dessertenne, Y. Cordier, M. A. DiForte-Poisson, S. L. Delage. *Eur. Phys. J. Appl. Phys.*, **2004**; *27*, 293.
[6] F. Cerdeira M. Cardona. *Phys. Rev. B*, **1972**; *5*, 1440.
[7] L. O'Reilly, K. Horan, P. J. McNally, N. S. Bennett, N. E. B. Cowern, A. Lankinen, B. J. Sealy, R. M. Gwilliam, T. C. Q. Noakes, P. Bailey. *Apply. Phys. Lett.*, **2008**; *92*, 233506.
[8] M. Becker, U. Gösele, A. Hofmann, S. Christiansen. *J. Appl. Phys.*, **2009**; *106*, 074515.
[9] T. S. Perova, B. M. Armstrong, J. Wasyluk, P. Baine, P. Rainey, S. J. N. Mitchell, D. W. McNeill, H. S. Gamble R. Hurley. *Solid St. Phenomena*, **2011**; *178–179*, 295.
[10] J. Wasyluk, P. V. Rainey, T. S. Perova, S. J. N. Mitchell, D. W. Mc-Neill, H. S. Gamble, B. M. Armstrong R. Hurley, J. Raman *Spectr.*, **2011**; *43*, 448.
[11] D. E. Aspnes A. A. Studna, *Phys. Rev. B*, **1983**; *27*, 985.
[12] A. Sanson, E. Napolitani, G. Impellizzeri, M. Giarola, D. De Salvadora, V. Privitera, F. Priolo, G. Mariotto, A. Carnera. *Thin Solid Films*, in print.
[13] E. Napolitani *et al*., *unpublished results*.
[14] G. Impellizzeri. E. Napolitani1, S. Boninelli, V. Privitera, T. Clarysse, W. Vandervorst, F. Priolo. *Appl. Phys. Express*, **2012**; *5*, 021301.
[15] The area of the Al-Ge Raman peak was calculated, after the background subtraction in the whole spectral range, as the integral between 360 and 380 cm^{-1} of the Raman spectrum with respect to the spectrum of pure Ge. The value of the Al-Ge peak intensity is influenced by the choice of the background subtraction method (which in our case is the same for all samples and laser lines). Nevertheless, we have verified that the linear trend of Fig. 2 was independent on the method of background subtraction used.
[16] J. Kim, S. W. Bedell, D. K. Sadana. *Appl. Phys. Lett.*, **2011**; *98*, 082112.
[17] H. Richter, Z.P. Wang, L. Ley. *Solid St. Comm.*, **1981**; *39*, 625.
[18] F. Cerdeira, C. J. Buchenauer, F. H. Pollak, M. Cardona. *Phys. Rev. B*, **1972**; *5*, 580.
[19] L. Romano, R. De Bastiani, C. Miccoli, G. Bisognin, E. Napolitani, D. De Salvador, M.G. Grimaldi. *Mat. Science and Engin. B*, **2006**; *135*, 220.
[20] G. Bisognin, S. Vangelista, M. Berti, G. Impellizzeri, M. G. Grimaldi. *J. Appl. Phys.*, **2010**; *107*, 103512.
[21] C. Y. Peng, C. F. Huang, Y. C. Fu, Y. H. Yang, C. Y. Lai, S. T. Chang, C. W. Liu. *J. Appl. Phys.*, **2009**; *105*, 083537.

